Abdul Satar, N. S., Adnan, R., Lee, H. L., Hall, S. R., Kobayashi, T., Mohamad Kassim, M. H., & Mohd Kaus, N. H. (2019). Facile green synthesis of ytrium-doped $BiFeO_3$ with highly efficient photocatalytic degradation towards methylene blue. *Ceramics International*, *45*(13), 15964-15973. https://doi.org/10.1016/j.ceramint.2019.05.105

Ceramics International xxx (xxxx) xxx–xxx

Contents lists available at ScienceDirect

Ceramics International

journal homepage: www.elsevier.com/locate/ceramint

Facile green synthesis of ytrium-doped $BiFeO_3$ with highly efficient photocatalytic degradation towards methylene blue

Nurul Syamimi Abdul Satar[a], Rohana Adnan[a], Hooi Ling Lee[a], Simon R. Hall[b], T. Kobayashi[c], Mohamad Haafiz Mohamad Kassim[d], Noor Haida Mohd Kaus[a,c,*]

[a] School of Chemical Sciences, Universiti Sains Malaysia, 11800, Penang, Malaysia
[b] Complex Functional Materials Group, School of Chemistry, University of Bristol, BS8 1TS, United Kingdom
[c] Department of Material Science and Technology, Nagaoka University of Technology, 1603-1 Kamitomioka, Nagaoka, 940-2188, Japan
[d] School of Industrial Technology, Universiti Sains Malaysia, 11800, Penang, Malaysia

ARTICLE INFO

Keywords:
Photocatalyst
Ceramic
Ytrrium-doped
Bismuth ferrite
Heterogeneous catalyst
Langmuir hinshelwood

ABSTRACT

Bismuth ferrite ($BiFeO_3$) is considered as one of the most promising materials in the field of multiferroics with great potentials in photocatalysis due to their excellent properties of relatively small band gap, stable structures, and low cost. In this work, a facile green route was successfully used for the fabrication of high-purity yttrium-doped and undoped bismuth ferrite ($BiFeO_3$) nanoparticles. κ-carrageenan seaweed was used as a biotemplate for the construction of the material. The obtained products were characterized and the photocatalytic effect of doped and undoped $BiFeO_3$ were evaluated on the degradation of methylene blue (MB) under direct sunlight. The formed particles are in the range of 80–90 nm that exhibited morphology of rhombohedral perovskite structure as confirmed by FESEM and HRTEM analysis. Decreasing of band gap energy from 2.07 eV to 2.05 eV as the concentration of yttrium dopant increased significantly affected their photocatalytic behaviour. There was a remarkable improvement in the photocatalytic activity of 1% of yttrium-doped $BiFeO_3$ towards the decomposition of methylene blue (MB) under direct sunlight irradiation. This was attributed to the strong absorption of visible light and the effective separation of photoinduced e− and h + pair, as compared to the pristine $BiFeO_3$. In addition, the influence of operational parameters on the removal efficiency of MB, such as catalyst dosage and initial dye concentrations, was optimized as a function of time. The kinetics of the photocatalytic MB removal was later found to follow Langmuir Hinshelwood model.

1. Introduction

Excessive amount of hazardous and toxic dyes being discarded into water streams results in pollution of the environment and significant health impacts on human beings [1]. During the recent years, heterogeneous photocatalyst has drawn considerable amount of attention as a green technique with its potential to eliminate and remove organic dyes from waste water. Furthermore, the emergence of various semiconductor photocatalysts, such as ZnO (3.18 eV) [2,3], TiO_2 (3.2 eV) [4,5] and CdS (2.34 eV) [6,7] has led to a marked progress in the field of heterogeneous visible-light photocatalysis. However, the main disadvantages of these semiconductors are the limitations of their photocatalytic activity in UV regions which limits the utilization of solar light since UV light represents less than 5% of solar light, photo corrosion or the rapid recombination of the photogenerated electron-hole pair. These result in the instability or less activity from the traditional photocatalysts under direct sunlight. Hence, it is necessary to develop a photochemically-stable photocatalyst and extend the photo response of materials to work efficiently under direct visible-light irradiation.

Among the vast majority of the metal oxide semiconductors, a rhombohedral distorted perovskite structure, which is known as $BiFeO_3$ nanoparticles, has received a significant amount of attention in the field of environmental remediation. This is due to its high photosensitivity at narrow band gap with high excitation binding energy, non-toxicity, and multiferroic properties at room temperature [5–8]. Since $BiFeO_3$ possesses narrow band gap energy, it is responsive to a wide spectrum of solar or visible light. Besides, its multiferroic behaviour is a contributing factor for the recyclability of a photocatalyst.

In order to overcome the problems of its poor reproducibility and poor ferroelectric behaviour that resulted from Bi volatilization, extensive works have been conducted in the synthesis of this chemical compound ensuring no impurities detected [9–11]. Additionally, higher

* Corresponding author. School of Chemical Sciences, Universiti Sains Malaysia, 11800, Penang, Malaysia.
E-mail address: noorhaida@usm.my (N.H. Mohd Kaus).

https://doi.org/10.1016/j.ceramint.2019.05.105
Received 20 December 2018; Received in revised form 27 April 2019; Accepted 10 May 2019

oxygen vacancy will affect the optical and photocatalytic properties of $BiFeO_3$. Nevertheless, the optical and photocatalytic properties of $BiFeO_3$ can substantially be improved by doping using rare earth metals [8,12,13] or transition elements [12]. Furthermore, the recombination of photogenerated electron-hole pairs could be inhibited by creating electron-hole trapping centre within the lattice of the photocatalyst. To illustrate this, several studies have reported that doping with rare earth metals, such as cerium (Ce) [13], strontium (Sr) [14], gadolinium (Gd) [15] and yttrium (Y) [16] will improve the optical properties as well as the photocatalytic activity of $BiFeO_3$ nanoparticles. Moreover, the enhancement of phase purity can also be achieved through the doping of metal elements between the A or B site of the materials. For example, Rai et al. [12] has reported that by substituting La^{3+} and Er^{3+} at the A-site of $BiFeO_3$, the perovskite phase is stabilized, and the volatilization of Bi ions and the number of oxygen vacancies are reduced.

Due to the recently growing interest in greener routes for the construction of functional materials, biotemplates are considered as good components for it. This is because they possess preferable chelation sites for the production of metal oxides nanoparticles. Recently [17], an anionic brown seaweed known as the κ-carrageenan, has been successfully utilised for directed growth of highly pure $BiFeO_3$ nanoparticles by employing facile biotemplated technique. In fact, introducing doping by rare earth metal could improve $BiFeO_3$'s photocatalytic efficiency by decreasing the particle size, increasing its surface area and subsequently narrowing the band gap. During the photocatalytic process, the dopant reduces the electron and hole pairs recombination by trapping the photoinduced electrons within the optimum level [18]. In this study, yttrium was chosen as the doping agent due to its smaller ionic radii (1.04 Å), in comparison to the bismuth, (1.17 Å). Therefore, yttrium may replace Bi^{3+} ions and result in the distortion and expansion of the lattice crystal structure [19]. In addition, the optical properties and photocatalytic activity of biotemplated yttrium-doped and undoped $BiFeO_3$ nanoparticles were explored. The main aim of this investigation was for the degradation of high concentration of methylene blue (MB) dye under direct sunlight irradiation. As a result, it was found that various percentages of yttrium dopant play an important role in photocatalytic performance, and the best composition was identified.

2. Experimental

2.1. Materials

The materials used for this investigation consisted of bismuth nitrate pentahydrate ($Bi(NO_3)_3.5H_2O$), iron nitrate nonahydrate ($Fe(NO_3)_3.9H_2O$), yttrium nitrate hexahydrate ($Y(NO_3)_3.6H_2O$) salts with a purity of more than 99%, and κ-carrageenan. These substances were obtained from Sigma-Aldrich. Meanwhile, hydrochloric acid (HCl) (37%), nitric acid (HNO_3) (96%), sodium nitrate ($NaNO_3$), and sodium hydroxide (NaOH) pellets were provided by R&M Chemicals. Methylene blue dye was purchased from QReC. Lastly, deionized water was used throughout this work.

2.2. Preparation of undoped and yttrium-doped $BiFeO_3$ nanoparticles

Firstly, $Bi(NO_3)_3.5H_2O$ and $Fe(NO_3)_3.9H_2O$ were weighed separately and mixed with a molar ratio of 1:1.7. prior dissolved in 25 mL deionized water. Next, 2.0 g of κ-carrageenan were dissolved in 100 mL of distilled water and the precursor was added into κ-carrageenan solution and stirred homogeneously, and the mixture was adjusted to pH 10 using NaOH (1.0 M). The mixture was heated at 80 °C under constant stirring for 2 h then dried in an oven overnight for the removal of the solvent. As the brown gel was obtained, it was calcined at 550 °C with a heating rate of 5 °C/min for 2 h. The synthesis of the yttrium-doped $BiFeO_3$ was slightly like the synthesis of undoped $BiFeO_3$, except that $Y(NO_3)_3.6H_2O$ was added into Bi–Fe ionic solution prior heating. Finally, the molarity of $Y(NO_3)_3.6H_2O$, that added into the Bi–Fe solution were varied with respect to the molarity of $Bi(NO_3)_3.5H_2O$.

2.3. Characterization of nanoparticles

The dried powders of the undoped and yttrium-doped $BiFeO_3$ nanoparticles were characterized through X-ray diffraction (XRD) analysis (Model BRUKER AXS D8 Advance X-ray diffractometer), which was conducted using Cu-Kα X-ray source and sodium iodide (NaI) scintillator type detector (λ = 1.5406 Å). The XRD patterns were recorded at 2θ value, which ranged from 20° to 80°. Furthermore, the sample morphology and chemical composition were examined using Scanning Electron Microscopy (FESEM, Zeiss Leo Supra 50 VP Oxford Instruments). This tool was equipped with an Energy Dispersive X-ray spectroscopy (EDX) microanalyzer (INCA-X, Oxford Instruments).

2.4. Degradation of MB under direct sunlight

The photocatalytic activities of undoped and yttrium-doped $BiFeO_3$ nanoparticles involved the investigation regarding the effects of catalyst dosage, MB initial concentration, kinetic study, and regeneration study. 50 mL of dye solution was transferred into a series of Erlenmeyer flasks. This was followed by the addition of catalyst dosage. Then, the dye mixture, which contained the photocatalyst, was left under direct sunlight during sunny days. The dates and duration taken for this process were between March to May, and for 3 h, which was between 10 a.m. and 3.00 p.m. There was no adjustment made on the pH value (pH 8). Between certain intervals, the solution was centrifuged, and the residual dye concentration was analyzed at 664 nm using a UV–Vis spectrophotometer. Lastly, a calculation was made on the amount of dye adsorbed using the following equation:

$$q_e = \frac{(C_o - C_e)V}{m} \quad (1)$$

Based on equation (1), q_e (mg/g) represents the amount of the dye adsorbed into the surface of solid materials. C_o and C_e (mg/L) represent the initial and the equilibrium concentrations of MB respectively. Meanwhile, V (L) represents the volume of MB taken for each run. On the other hand, m (g) represents the mass of the absorbent added into the solution. The removal efficiency of the dye was determined by following equation (2) [20]:

$$Removal\ (\%) = \frac{(C_o - C_e)100}{C_o} \quad (2)$$

From this equation, C_o and C_e (mg/L) are the same labels for the parameters mentioned above. The experiments were conducted in triplicates and the average values were used.

3. Results and discussion

3.1. Structural analysis of Y-doped and undoped $BiFeO_3$

The XRD pattern of the yttrium-doped $BiFeO_3$ (Y-doped $BiFeO_3$), which was synthesized using 2.0% of w/v κ-carrageenan was obtained and compared to those of the pristine samples as presented in Fig. 1. From the result obtained, both X-ray diffraction patterns displayed similar peaks corresponding to the high purity of $BiFeO_3$, regardless of the amount of yttrium dopant added. An interesting finding of this experiment was that the peak level of intensity at [110] plane decreased with the increasing amount of Y dopant. This observation may have resulted from the reduction of bismuth content, which was followed by doping with yttrium ion. Furthermore, the volatilization of Bi^{3+} ions created vacancy at A site, which led to this doping. It was indicated from the changes in the intensity of the corresponding peak at [110] that there was a reduction in the particle size of the rhombohedral phase, as the percentage of dopant Y increased [16]. An exception was

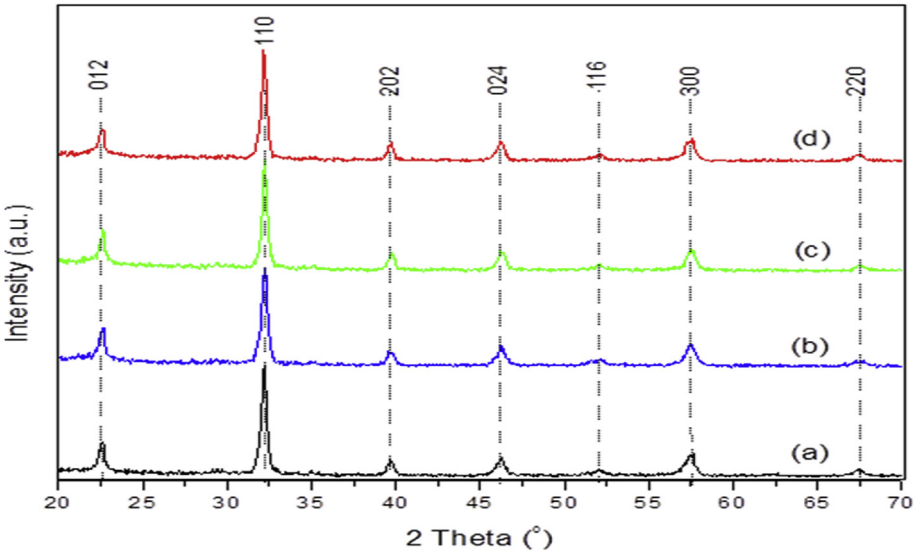

Fig. 1. XRD patterns of undoped and Y-doped $BiFeO_3$ nanoparticles; (a) undoped, (b) 5%, (c) 2% and (d) 1% of Y-doped.

Table 1
Comparison of crystallite size, particle size, BET surface area, and band gap energy of undoped and Y-doped $BiFeO_3$.

Sample	Crystallite size at [110] plane (nm)	Particle size (nm)	BET surface area (m^2/g)	Band gap (eV)
Undoped $BiFeO_3$	14	97 ± 21	8.86	2.07
1% Y–$BiFeO_3$	14	90 ± 14	10.78	2.14
2% Y–$BiFeO_3$	14	104 ± 12	10.19	2.08
5% Y–$BiFeO_3$	14	129 ± 42	6.47	2.05

regarding the decrease in the [110] crystalline peak as it is the preferential crystallographic growth and orientation along that direction. However, the introduction of dopant Y to $BiFeO_3$, did not affect the crystallite size, (Table 1).

3.2. Morphological and surface area analysis of Y-doped and undoped $BiFeO_3$

FESEM images in Fig. 2 indicate that the morphology of Y-doped $BiFeO_3$ had a rhombohedral shape with smaller particle sizes compared to the morphology of the undoped nanoparticles. The decrease in the grain size of the nanoparticles was attributed to the densification of Y^{3+}, which occupied the Bi^{3+} positions [16]. The particle size distributions and the standard deviation of the undoped and the Y-doped $BiFeO_3$ nanoparticles, which were prepared using 2.0% of w/v κ-carrageenan were presented in Table 1. The average particle sizes of the undoped, which were 1%, 2%, and 5% of Y-doped $BiFeO_3$, were determined to be 96.8 ± 21, 89.7 ± 14, 104.3 ± 12, and 129.3 ± 42 nm, respectively.

Various surface area (S_{BET}) of undoped and Y-doped $BiFeO_3$ nanoparticles in the presence of 2% of w/v κ-carrageenan was followed by the trend of 1% of Y-doped > 2% of Y-doped > undoped > 5% of Y-doped. Furthermore, the addition of a small amount of yttrium increased the surface area of the sample, due to the formation and distribution of the smaller particles, as shown in the FESEM analysis (Fig. 2). The addition of 1% yttrium on $BiFeO_3$ reducing the particle size which in turn provides high surface area for active sites. This is due to the "grain growth inhibition" effect of the dopant. It will be lowering the grain size of particles as dopants often act to pin grain boundaries and therefore limit the grain boundary mobility. Concentration of maximum dopant increases with surface to volume ratio of the grain and it is higher for nanosized grains. Above a given concentration of 1% of yttrium, a new (dopant-rich) phase precipitates. Precipitation occurs at lower dopant concentrations as grain size increases lead to larger crystals obtained. Theoretically, the surface area of the samples will affect the photocatalytic activity. Therefore, it was hypothesized that the photocatalysts with smaller particle sizes will render high photocatalytic performance [21,22].

Besides, the band gap energy of the samples will be affected by the photocatalysts with this particle size. The inverse relationship between particles' size and band gap was expected, as smaller particles had larger surface area that illustrated in Table 1.

3.3. Optical properties of Y-doped and undoped $BiFeO_3$

Based on Fig. 3, it is shown that the band gap energy was determined based on the extrapolation of tangent line through the point of inflection in diffuse reflectance spectroscopy absorption band. The addition of yttrium in the synthesis of $BiFeO_3$ nanoparticles altered the band gap energy of the nanoparticles (Table 1). The value of the band gap energy decreased as the amount of yttrium increased. The decrease in the band gap energy correlated with the decrease in the surface area of $BiFeO_3$ samples. As evidence, the smallest band gap energy was owned by 5% of Y-doped $BiFeO_3$, which also possessed the lowest surface area among all the tested samples. A plausible explanation for this effect was that the bulk defects induced a delocalization of the conduction band edge. Other than that, the defects created shallow traps in electronic energy, causing a red shift in the absorption spectra [28]. Moreover, the decrease in the band gap value can also be ascribed to the reduction of oxygen vacancies, which were located at BO_6. It is also ascribed to the suppressed tilt angle of the oxygen octahedral, which increased the Fe–O–Fe angle [23]. This phenomenon also explained the larger band gap energy of 1% of Y–$BiFeO_3$ in comparison to that of the undoped $BiFeO_3$. This is because the former sample had smaller particle sizes, which rendered a higher surface area. From the calculated band gap, it can be predicted that these nanoparticles can be applied as photocatalyst in the degradation of dyes and organic molecules under visible light.

3.4. FTIR spectra of Y-doped and undoped $BiFeO_3$

In Fig. 4, the FTIR spectra, which corresponded to the samples prepared in the presence of yttrium, was recorded within the range of 400–4000 cm^{-1}. The fundamental absorption band for $BiFeO_3$ was found within the range of 400–700 cm^{-1}. This corresponded to Fe–O

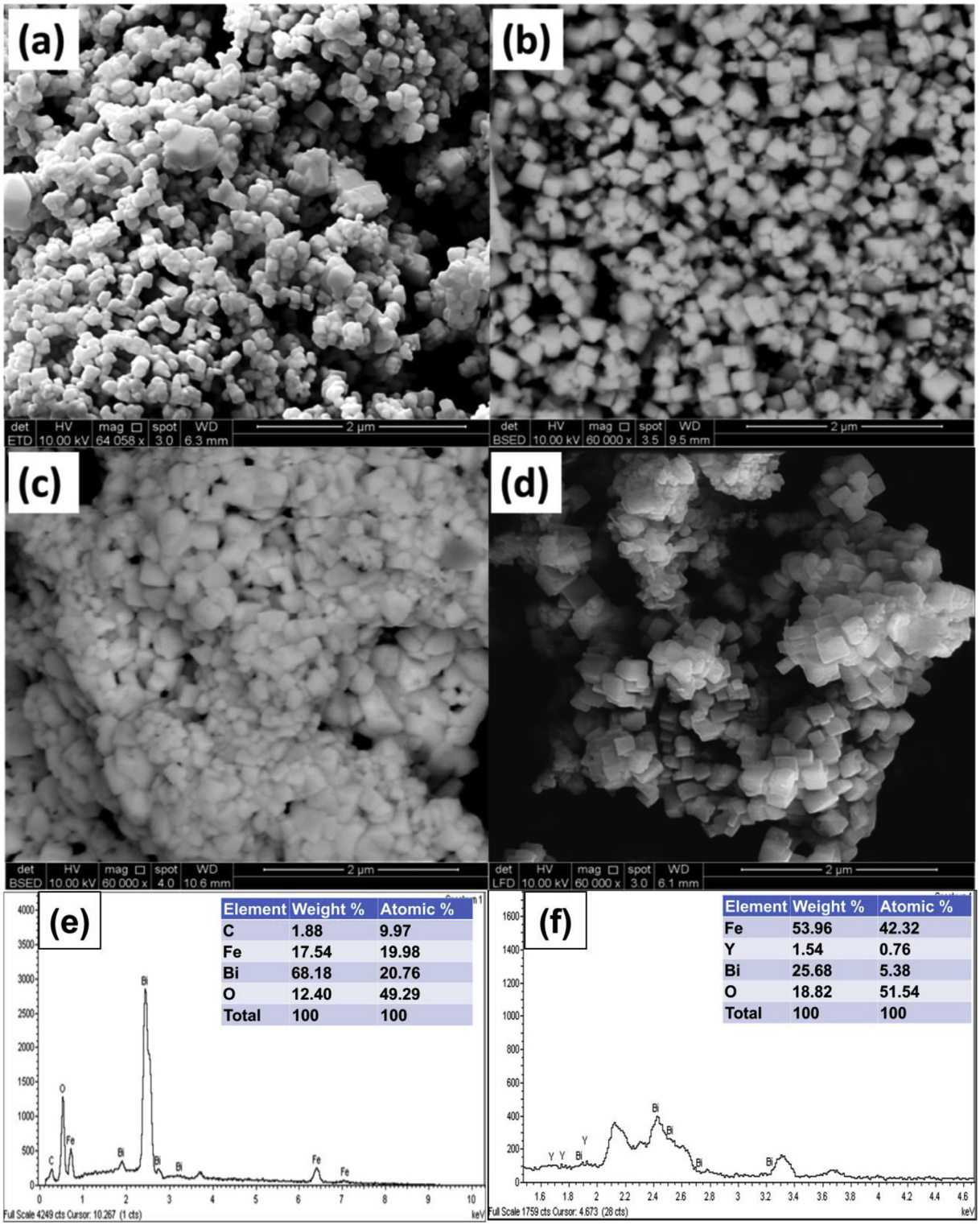

Fig. 2. FESEM images and EDX of undoped and Y-doped $BiFeO_3$ nanoparticles; (a) undoped, (b) 1%, (c) 2% (d) 5% of Y-doped, (e) EDX of undoped and (f) EDX of Y-doped $BiFeO_3$.

and Bi–O bond vibrations [24]. Furthermore, the Fe–O bending and stretching vibrations in the perovskite structure, which implied the formation of $BiFeO_3$, were observed at 420 cm^{-1} due to the internal vibration of FeO_6 octahedra [8]. Moreover, the absorption band, which ranged from 500 to 650 cm^{-1} in Fig. 4, was assigned to Bi–O stretching vibration in the strongly distorted BiO_6 octahedral units. In addition, at 880 cm^{-1}, the absorption band was originated from the symmetric stretching vibrations of O–Bi–O in pyramidal BiO_3 units [24]. It was shown by the FTIR spectra of the Y-doped samples that Bi–O, Fe–O, and O–Fe–O bands were slightly shifted towards the lower wavenumber from 592 to 570 cm^{-1}. The changes might be due to the structural distortion, as discussed earlier in FESEM and XRD analyses.

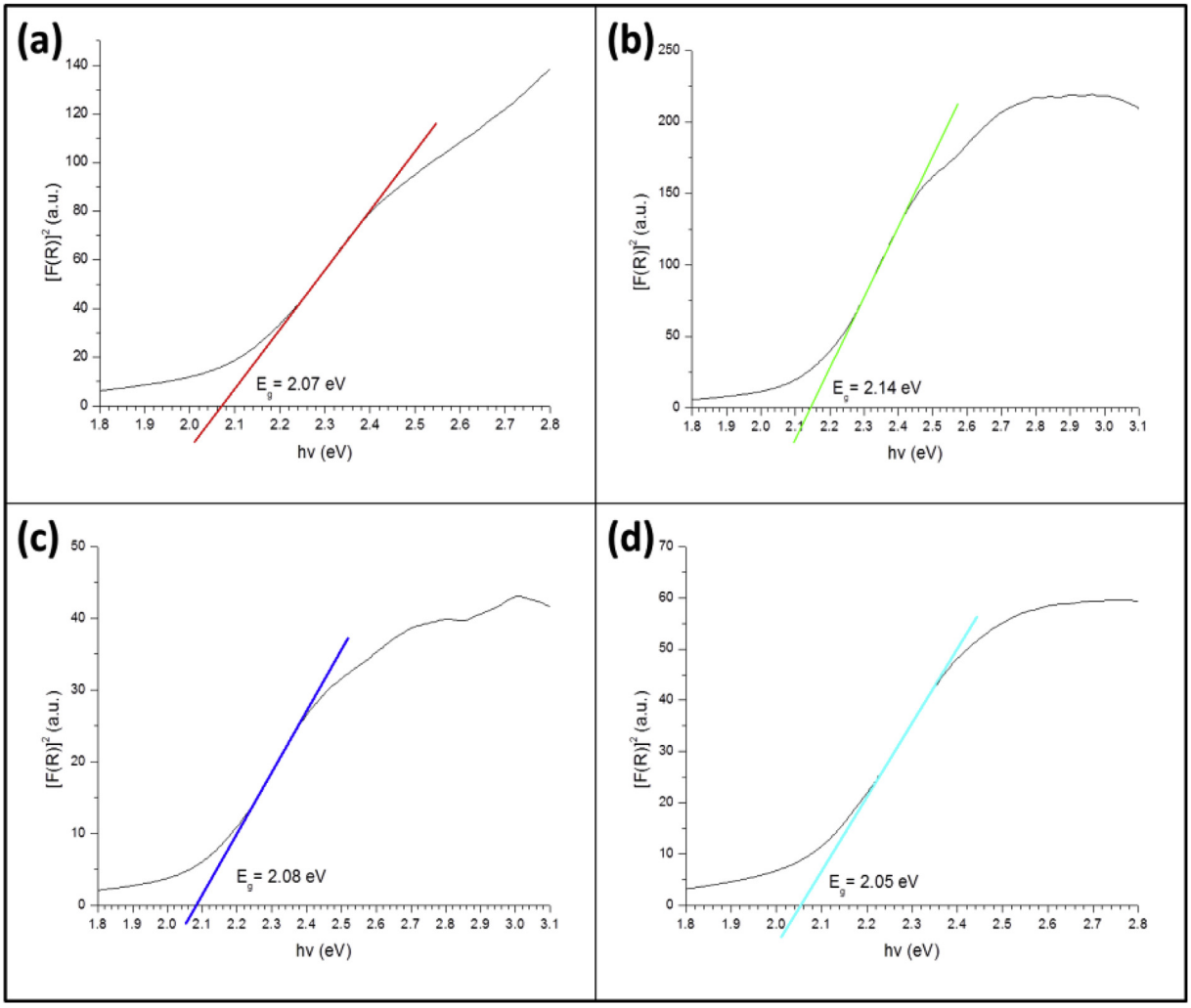

Fig. 3. Direct band gap energy of (a) undoped, (b) 1%, (c) 2% and (d) 5% Y-doped $BiFeO_3$ nanoparticles.

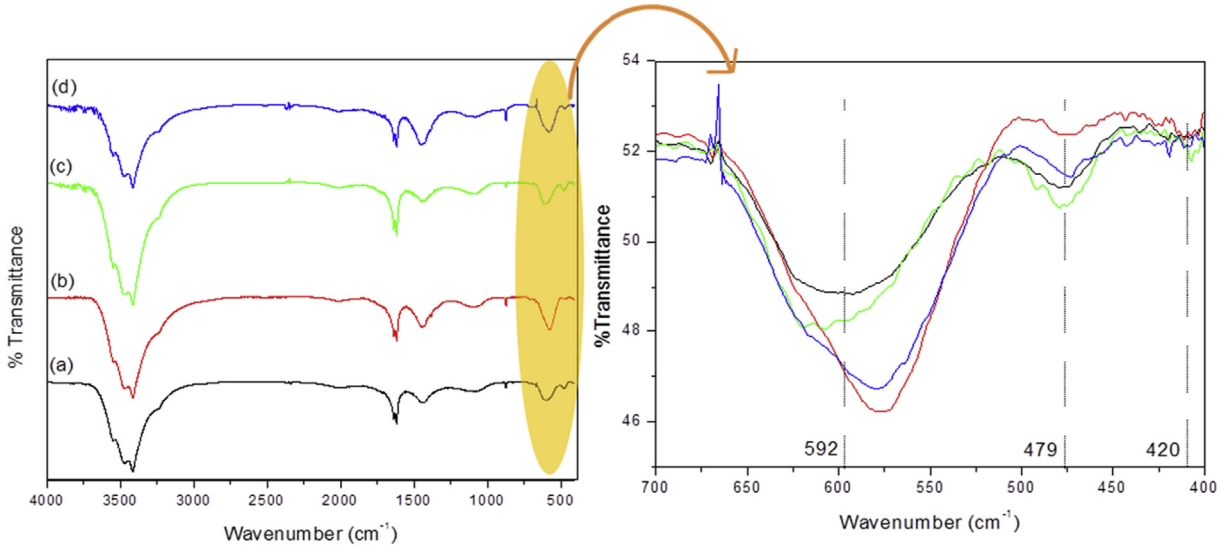

Fig. 4. FTIR spectra of (a) undoped and Y-doped $BiFeO_3$ (b) 1%, (c) 2% and (d) 5% of Y-doped, which were prepared at pH 10 with Bi:Fe molar ratio of 1:1.7 using 2% of w/v κ-carrageenan, and calcined at 550 °C for 2 h.

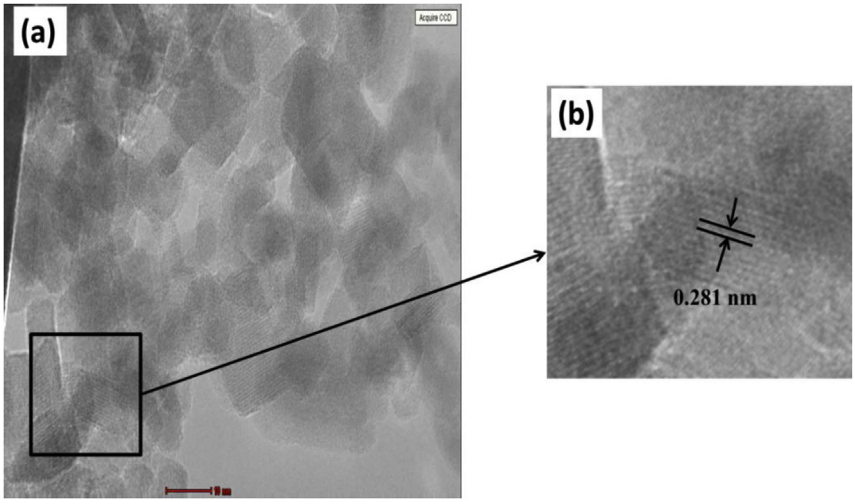

Fig. 5. (a) HRTEM image, and (b) d-value interplanar spacing calculation of $BiFeO_3$ nanoparticles prepared at pH 10 with Bi:Fe molar ratio of 1:1.7 using 2% w/v κ-carrageenan and calcined at 550 °C for 2 h.

3.5. High-resolution transmission electron microscopy (HRTEM)

HRTEM image of the selected area of $BiFeO_3$ nanoparticles was obtained to confirm the crystallinity and lattice spacing of the as-prepared $BiFeO_3$ sample. As illustrated in Fig. 5, the interplanar spacing corresponding to the [110] plane of the sample calcined at 550 °C was found to be 0.281 nm and this value is in correlation with the experimental findings from the XRD analysis. These results further confirmed the formation of high purity $BiFeO_3$ nanoparticles with high purity in the synthesize $BiFeO_3$ in the presence of κ-carrageenan.

3.6. Magnetic properties

To investigate the magnetic properties of the prepared $BiFeO_3$ nanoparticles, the magnetic hysteresis (M − H) loop of $BiFeO_3$ was measured at room temperature and the result is shown in Fig. 6. $BiFeO_3$ is an antiferromagnetic system but it shows ferromagnetic properties at room temperature [31]. The result confirmed that the $BiFeO_3$ nanoparticles exhibited ferromagnetic ordering, as evidenced by the magnified view of the M − H curves at lower applied field [29] which showed that hysteresis appeared with a residual magnetic moment of 8.83×10^{-2} emu/g and coercive field of 79.95 Oe when applied with a magnetic field of 20 kOe. Nevertheless, the remnant magnetization of this material is higher than that observed by Ref. [30], who reported the value of 6.70×10^{-2} emu/g which may be attributed to the smaller particle sizes of the nanoparticles produced.

3.7. Point of zero charge (PZC)

The pH level of point of zero charge (pH_{PZC}) can be defined as the pH level at which there is no net charges on the surface of the sample [25]. Determining the pH_{PZC} of the sample is crucial; in order to obtain the amount of charges made on the surface of the sample at different pH levels. At this point, it is essential to estimate the optimum pH level for the degradation of MB. Furthermore, it was shown from the results that the pH_{PZC} of undoped, which amounted to 1%, 2%, and 5% of Y-doped $BiFeO_3$ ranged between 8.4 and 8.8. In the event where the pH value of the solution was lower than pH_{PZC}, the surface of the sample was positively charged, and the sites were protonated. This was due to the excess H^+ surrounding the surface of the photocatalyst. On the other hand, when the pH level of the solution was higher than pH_{PZC}, the surface of the photocatalyst became negatively charged. Additionally,

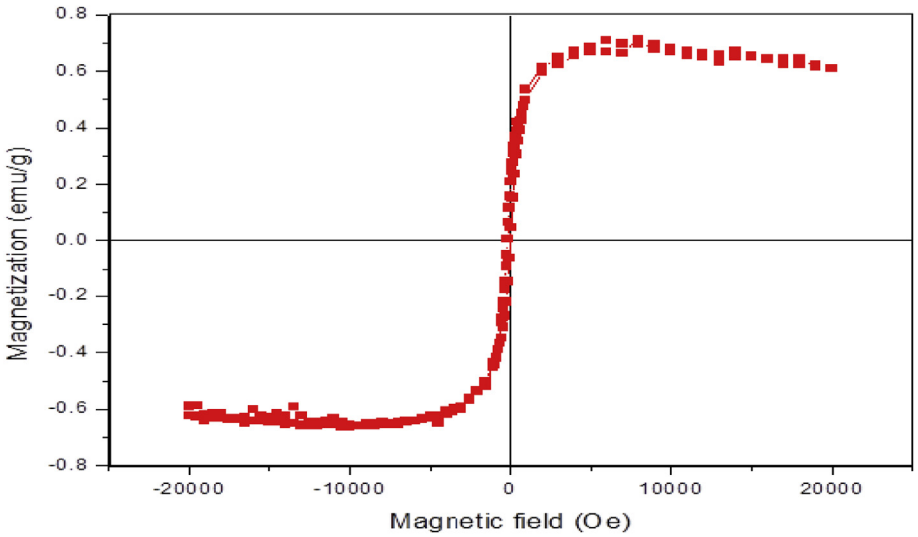

Fig. 6. M–H loop curve of BiFeO3 nanoparticles prepared at pH 10 with Bi:Fe molar ratio of 1:1.7 using 2% w/v κ-carrageenan and calcined at 550 °C for 2 h measured at room temperature.

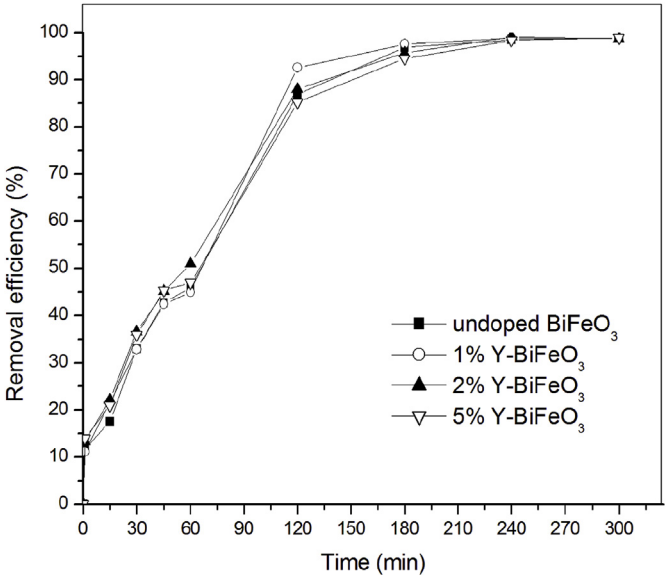

Fig. 7. The effects of irradiation time on the removal of MB in aqueous solution, using undoped and Y-doped $BiFeO_3$ ($[MB]_o$ = 50 mg/L, 0.1 g catalyst and at unadjusted pH).

the site had excess ^{-}OH ions, which could be counter-balanced by H^+ molecule, which was fred from the photocatalyst surface.

3.8. Photocatalytic activity on methylene blue dye

The undoped and Y-doped $BiFeO_3$, were prepared in the presence of 2% of w/v κ-carrageenan, were validated for the degradation of methylene blue under sunlight. The validation was conducted through various operational parameters, such as reaction time, catalyst dosage, and the initial concentration of MB. It was expected that a good catalyst exhibited high adsorption rate and capacity. In general, the rate of photocatalytic activity was found to be faster at the beginning due to the freely available active sites on the surfaces. However, the rate of photocatalytic activity eventually became slower when the surfaces became saturated. Furthermore, there was no further increase observed in the removal efficiency of dye (MB) when the equilibrium state was established. As discussed earlier, the effects of yttrium dopant in the synthesized $BiFeO_3$ nanoparticles resulted to a notable improvement in the particles' size, surface area, and band gap energy. Therefore, it was predicted that the Y-doped $BiFeO_3$ will render better photocatalytic performance, in comparison to the photocatalytic performance of the undoped $BiFeO_3$. The effects of contact time on the photocatalytic degradation of MB by the Y-doped $BiFeO_3$, which were prepared in the presence of 2% w/v κ-carrageenan, were studied, and the result is presented in Fig. 7.

1% and 2% of Y-doped $BiFeO_3$ exhibited better removal efficiencies, as compared to the removal efficiencies displayed by the undoped $BiFeO_3$ as presented in Table 2. At the 120 min, 92.6 and 88.0% of MB

Table 2
The removal efficiency of MB at 120 and 180 min using undoped and Y-doped $BiFeO_3$, which were prepared using 2% of w/v κ-carrageenan ($[MB]_o$ = 50 mg/L, 0.1 g catalyst and at unadjusted pH).

Sample	Removal efficiency (%)	
	120 min	180 min
Undoped $BiFeO_3$	87.0 ± 0.2	96.6 ± 0.1
1% Y–$BiFeO_3$	92.6 ± 0.1	97.6 ± 0.1
2% Y–$BiFeO_3$	88.0 ± 0.1	95.7 ± 1.7
5% Y–$BiFeO_3$	85.2 ± 0.2	94.5 ± 0.1

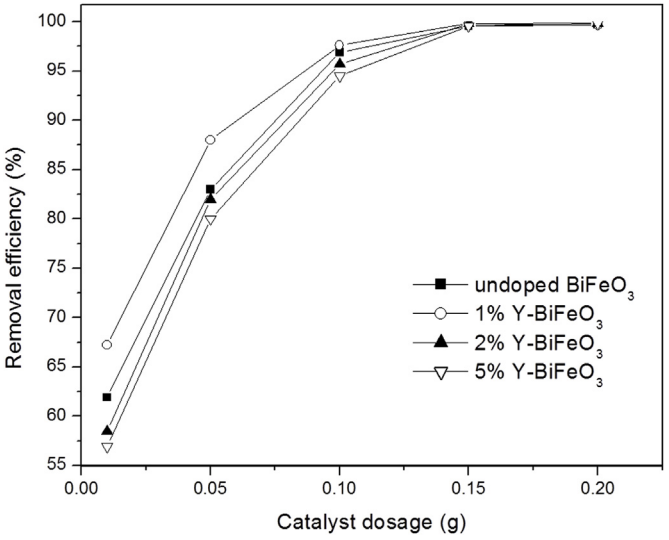

Fig. 8. The effects of catalyst dosage on the removal efficiency MB ($[MB]_o$ = 50 mg/L, for 180 min under direct sunlight at unadjusted pH).

were removed by 1% and 2% of Y-doped $BiFeO_3$ respectively. On the other hand, the removal efficiency for the undoped catalyst was 87.0%, which was slightly lower. However, as the duration was extended to 180 min, a comparable removal efficiency was observed for 1%, 2% of Y-doped, and undoped $BiFeO_3$, which amounted to 97.6, 95.7, and 96.9, respectively. Nevertheless, 5% of Y-doped $BiFeO_3$ exhibited a slight decrease in the MB removal, with 85.2% of MB removed in 120 min. In addition, 94.5% of MB was removed in 180 min. This outcome might be attributed to the lower surface area of the 5% of Y-doped $BiFeO_3$ (6.47 m^2/g), which corresponded to the less active sites for the interaction between the surface of the photocatalyst and the MB molecules.

To determine the effects of catalyst dosage, optimum amount of materials was investigated at an unadjusted pH level (pH 8) by varying the amount of catalyst from 0.01 to 0.20 g at fixed MB solution concentration, 50 mg/L. At an initial dose of 0.01 g, the MB removal efficiency of undoped, 1%, 2%, and 5% of Y-doped $BiFeO_3$ samples were amounted to 61.9, 67.2, 58.5 and 56.9%, respectively as displayed in Fig. 8. The percentage was further enhanced to 99% as the catalyst dosage was increased to 0.2 g. The improvement can be explained due to the increase in the number of active sites as the amount of the catalyst increase [23]. The optimum amount of the catalyst for MB degradation of 99% was 0.1 g for the 1% Y-doped $BiFeO_3$, while the undoped, 2% and 5% Y-doped $BiFeO_3$ required a slightly higher dosage of 0.15 g to show similar MB removal efficiency. In other words, it can be concluded that the MB removal efficiency by 1% Y-doped $BiFeO_3$ was significantly higher as compared to that of the other three samples.

The effect of the initial concentration of MB (Fig. 9) was studied within the range between 30 and 100 mg/L, in 180 min. This study was conducted under direct sunlight without adjusting the pH level with the optimum catalyst dosage, which was 0.1 g. At a low concentration level, more MB was absorbed, as most of the active sites were unoccupied. As the amount of MB increased, more MB molecules were absorbed into the surface of the photocatalyst. However, there was a decrease in the number of available active sites and a continuous increase in the amount of MB molecules in the MB initial concentration. The increase went on until it reached the maximum saturation level and the decrease of removal efficiency [26].

From Figs. 9 and 100% degradation of MB was obtained through 1% of Y-doped $BiFeO_3$ with a concentration level up to 50 mg/L. Meanwhile, 100% degradation obtained by undoped, 2% of Y-doped, and 5% of Y-doped $BiFeO_3$ were at 40 mg/L. However, the removal efficiency was reduced to 61%, when MB's initial concentration increased further to 100 mg/L. This indicated that at a higher MB concentration, there

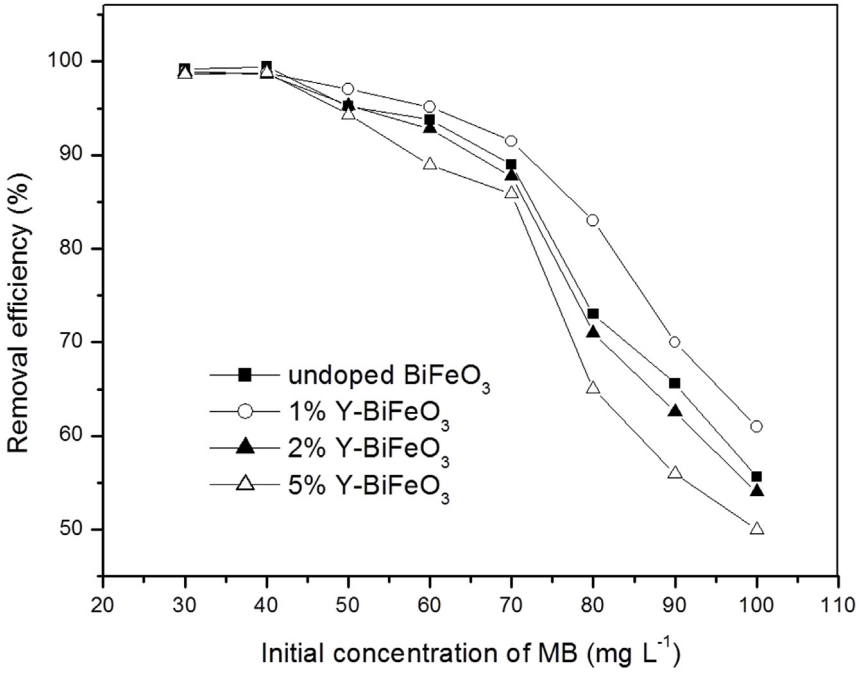

Fig. 9. The effects of the initial concentrations of MB on the removal efficiency of MB (180 min under direct sunlight, 0.1 g catalyst, unadjusted pH).

Table 3
The rate constants and correlation coefficients, R^2, for the degradation of MB in aqueous solution by undoped and Y-doped $BiFeO_3$, which were prepared in the presence of 2% of w/v κ-carrageenan. ($[MB]_o$ = 50 mg/L, 0.1 g catalyst and at unadjusted pH).

Sample	Rate constant, k (min^{-1})	Correlation coefficients, R^2
Undoped $BiFeO_3$	0.0163	0.989
1% Y–$BiFeO_3$	0.0170	0.979
2% Y–$BiFeO_3$	0.0164	0.988
5% Y–$BiFeO_3$	0.0163	0.981

was an increase in the amount of catalyst surface needed. However, in this study, since the irradiation time and catalyst dosage were constant, there was a consistency in the $OH^{\bullet}$ radicals, even though the MB concentration increased. Therefore, there were an insufficient number of free radicals required to prevent the increasing number of MB molecules, as the concentration increased [27].

3.9. Kinetic model

Langmuir–Hinshelwood (LH) kinetics model is the most commonly used kinetic expression to illustrate the kinetics of heterogeneous photocatalytic processes. The reaction of kinetics was expressed using

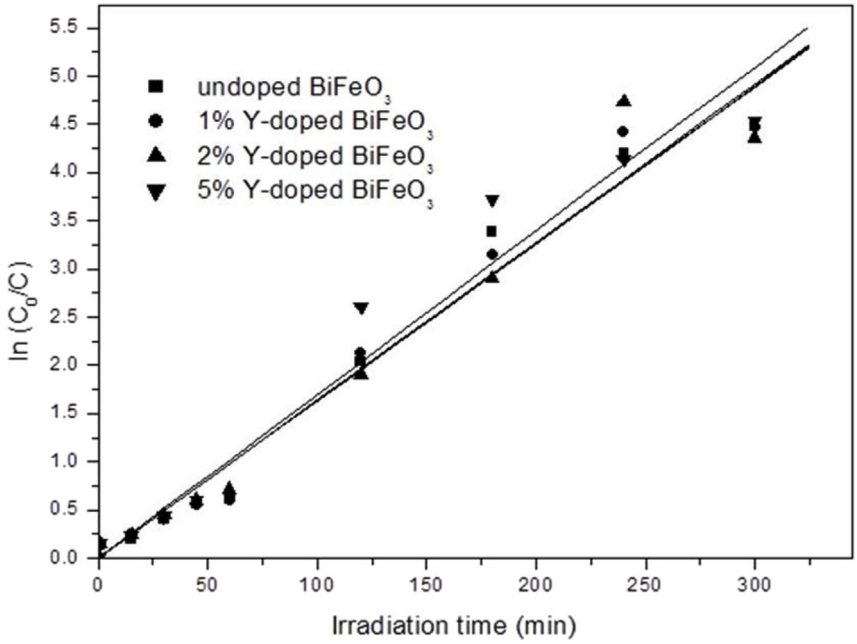

Fig. 10. Langmuir Hinshelwood's kinetic model of undoped and Y-doped $BiFeO_3$, which was prepared in the presence of 2% of w/v κ-carrageenan ($[MB]_o$ = 50 mg/L, 0.1 g catalyst and at unadjusted pH).

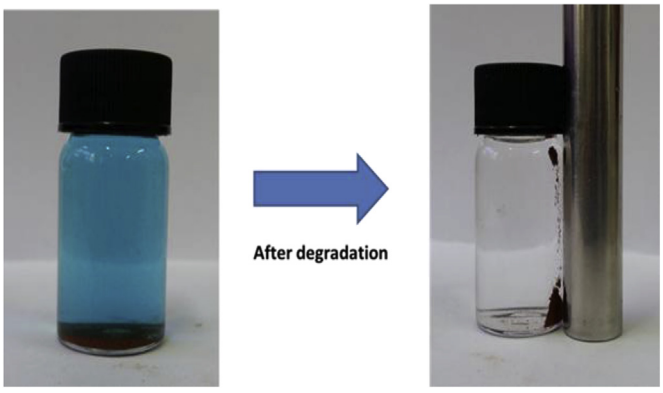

Fig. 11. The recovery of $BiFeO_3$ nanoparticles using a magnet after degradation of 50 mg/L of MB for by using 0.1 g catalyst after 180 min under direct sunlight.

equation (3):

$$ln\frac{C_0}{C} = kt \tag{3}$$

Based on this equation, C_0 (mg/L), C (mg/L), and k (min^{-1}) represent the dye concentration at time t = 0 min, t (minute), and the first-order rate constant, respectively. The rate constant, can be obtained through a linear fit from the plot of ln C_0/C versus irradiation time. Then, the results are summarized in Table 3 and Fig. 10. Based on the results, the addition of 1% of dopant Y to $BiFeO_3$ in the presence of 2% of w/v κ-carrageenan significantly improved the rate of the photocatalytic degradation of MB. This process was a first order reaction. 1% of Y-doped $BiFeO_3$ nanoparticles exhibited the highest photocatalytic degradation rate, with k value of 0.0170 min^{-1}. Lastly, this result ascribed to its smaller particles size (89.7 nm), and the larger surface area, as discussed earlier in Section 3.1.

3.10. Recyclability of Y-doped and undoped $BiFeO_3$

Further examination was made on the stability and recyclability of the undoped and Y-doped $BiFeO_3$ nanoparticles to ensure the materials remained active for the next photocatalytic degradation cycle. In this case, after the reaction was completed, the catalyst was separated from the treated MB solution using an external magnet (Fig. 11). The catalyst was then reused for the next photocatalytic reaction.

It is shown by the results in Fig. 12 that the removal efficiencies of the undoped and Y-doped $BiFeO_3$ nanoparticles remained above 90% up to 4 consecutive cycles. However, the removal efficiencies of Y–$BiFeO_3$ remained 5%, which was lower. These results demonstrated that the prepared undoped and Y-doped $BiFeO_3$ had excellent potential as photocatalyst under visible light. This is because they could be repeatedly used with an added advantage, which referred to the easy separation of the catalyst. At the fifth cycle, the removal efficiency decreased, to the point that it was close to 60%. This loss in efficiency may be due to the weakening of the absorption capability of the catalysts, or the leaching of the catalysts into the reaction medium during the recovery process.

4. Conclusion

In conclusion, undoped and Y-doped $BiFeO_3$ nanoparticles were successfully synthesized using green and facile biotemplated technique. Y-doped $BiFeO_3$, with varying amount of dopant Y, consisted of different morphology and optical properties. As compared to the undoped $BiFeO_3$ with 96 nm particle size, the particle size of 1% of Y-doped $BiFeO_3$ was found to be 85 nm. The band gap energy of undoped $BiFeO_3$ increased from 2.07 to 2.14 eV when 1% of Y dopant was added to produce 1% of Y-doped $BiFeO_3$. Furthermore, the total surface area of $BiFeO_3$ also increased from 8.86 to 10.78 m^2/g with the inclusion of 1% of Y dopant. There was a significant improvement shown by Y-doped $BiFeO_3$ in photocatalytic activities. This is because 1% of Y-doped $BiFeO_3$ nanoparticles exhibited better photocatalytic efficiency, in comparison to the undoped $BiFeO_3$. This is where Y-doped $BiFeO_3$ required less photocatalyst dosage (0.1 g) and shorter irradiation time (120 min). Moreover, the experiment showed that $BiFeO_3$ photocatalysts were highly recyclable up to four consecutive cycles without risking significant loss of their photocatalytic efficiencies. Besides, they had the potential to be utilised as an efficient photocatalyst, to remove various organic dyes and pollutants under naturally available sunlight.

Acknowledgement

This work was supported by Universiti Sains Malaysia in the form of Research University Grant Scheme (1001/PKIMIA/811249) and (1001/

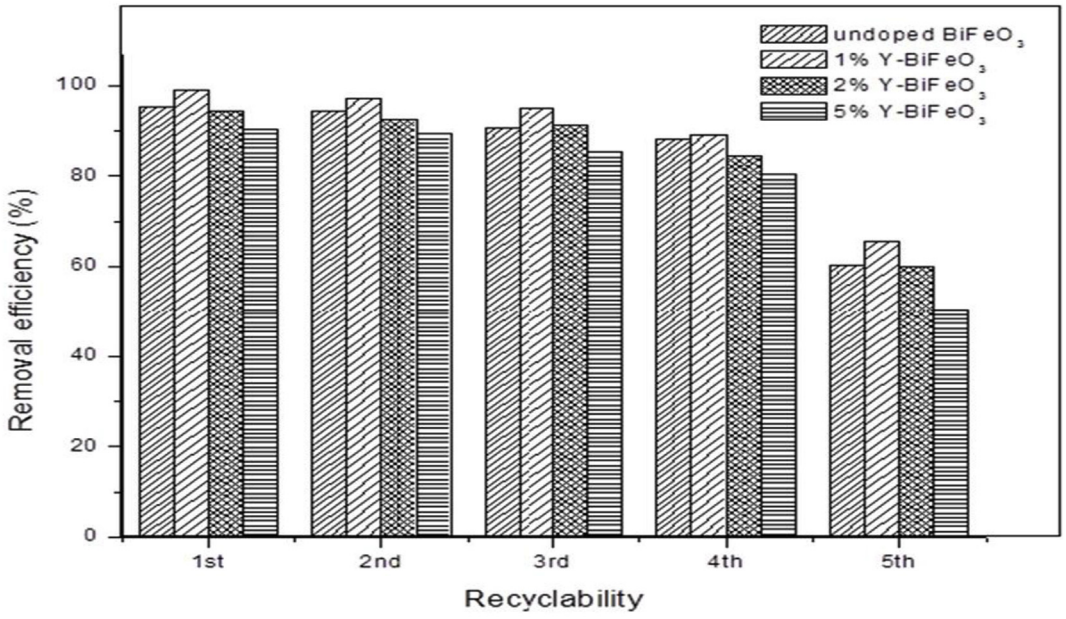

Fig. 12. The recyclability of undoped and Y-doped $BiFeO_3$ ($[MB]_o$ = 50 mg/L, 0.1 g catalyst for 180 min under direct sunlight at unadjusted pH).

PKIMIA/8011069).

Abbreviation

A	Absorbance
M	Molar
Mb	Methylene blue
pH_{pzc}	pH of point of zero charge
Y-doped	Yttrium doped

References

[1] G. Catalan, J.F. Scott, Physics and applications of bismuth ferrite, Adv. Mater. 21 (2009) 2463–2485.

[2] M. Soltaninezhad, A. Aminifar, Study nanostructures of semiconductor zinc oxide (ZnO) as a photocatalyst for the degradation of organic pollutants, Int. J. Nano Dimens. (IJND) 2 (2) (2011) 137–145.

[3] U. Alam, A. Khan, W. Raza, A. Khan, D. Bahnemann, M. Muneer, Highly efficient Y and V co-doped ZnO photocatalyst with enhanced dye sensitized visible light photocatalytic activity, Catal. Today 284 (2017) 169–178.

[4] C. Guillard, H. Lachheb, A. Houas, M. Ksibi, E. Elaloui, J.M. Herrmann, Influence of chemical structure of dyes, of pH and of inorganic salts on their photocatalytic degradation by TiO2comparison of the efficiency of powder and supported TiO2, J. Photochem. Photobiol. A Chem. 158 (2003) 27–36.

[5] B. Li, C. Wang, W. Liu, M. Ye, N. Wang, Multiferroic properties of La and Mn co-doped BiFeO3nanofibers by sol-gel and electrospinning technique, Mater. Lett. 90 (2013) 45–48.

[6] G. Guan, T. Kida, K. Kusakabe, K. Kimura, E. Abe, A. Yoshida, Photocatalytic activity of CdS nanoparticles incorporated in titanium silicate molecular sieves of ETS-4 and ETS-10, Appl. Catal. Gen. 295 (2005) 71–78.

[7] X. Li, C. Hu, X. Wang, Y. Xi, Photocatalytic activity of CdS nanoparticles synthesized by a facile composite molten salt method, Appl. Surf. Sci. 258 (2012) 4370–4376.

[8] A. Mukherjee, S. Basu, L.A.W. Green, N.T.K. Thanh, M. Pal, Enhanced multiferroic properties of Y and Mn codoped multiferroic BiFeO3nanoparticles, J. Mater. Sci. 50 (2015) 1891–1900.

[9] R. Safi, H. Shokrollahi, Physics, chemistry and synthesis methods of nanostructured bismuth ferrite (BiFeO3) as a ferroelectro-magnetic material, Prog. Solid State Chem. 40 (2012) 6–15.

[10] B. Sanyal, O. Eriksson, Advanced Functional Materials: A Perspective from Theory and Experiment, Elsevier Science, Oxford, 2012.

[11] J. Silva, A. Reyes, H. Esparza, H. Camacho, L. Fuentes, BiFeO3: a review on synthesis, doping and crystal structure, Integr. Ferroelectr. 126 (2011) 47–59.

[12] R. Rai, S.K. Mishra, N.K. Singh, S. Sharma, A.L. Kholkin, Preparation, structures, and multiferroic properties of single-phase BiRFeO3, R = la and Er ceramics, Curr. Appl. Phys. 11 (2011) 508–512.

[13] M. Tokunaga, M. Akaki, T. Ito, S. Miyahara, A. Miyake, H. Kuwahara, N. Furukawa, Magnetic control of transverse electric polarization in BiFeO3, Nat. Commun. 6 (2015) 1–5.

[14] B. Bhushan, A. Basumallick, N.Y. Vasanthacharya, S. Kumar, D. Das, Sr induced modification of structural, optical and magnetic properties in Bi1-xSrxFeO3(x = 0, 0.01, 0.03, 0.05 and 0.07) multiferroic nanoparticles, Solid State Sci. 12 (2010) 1063–1069.

[15] Z.X. Cheng, X.L. Wang, S.X. Dou, H. Kimura, K. Ozawa, Enhancement of ferroelectricity and ferromagnetism in rare earth element doped BiFeO3, J. Appl. Phys. 104 (2008) 1–4.

[16] A. Mukherjee, S.M. Hossain, M. Pal, S. Basu, Effect of Y-doping on optical properties of multiferroics BiFeO3 nanoparticles, Appl. Nanosci. 2 (2012) 305–310.

[17] N.S. Abdul Satar, W.A. Aziz, M.K. Yaakob, M.Z.A. Yahya, O.H. Hassan, T.I.T. Kudin, N.H. Mohd Kaus, J. Phys. Sci. 120 (2016) 26012–26020.

[18] C. Kaan, A. Aziz, S. Ibrahim, Heterogeneous photocatalytic oxidation an effective tool for wastewater treatment–A review, Stud. Water Manag. Issues 9 (2012) 1–274.

[19] M. Kumar Trivedi, Studies of the atomic and crystalline characteristics of ceramic oxide nano powders after bio field treatment, Ind. Eng. Manag. 04 (2015).

[20] L. Hou, L. Yang, J. Li, J. Tan, C. Yuan, Efficient sunlight-induced methylene blue removal over one-dimensional mesoporous monoclinic BiVO4nanorods, J. Anal. Methods Chem. 1 (2012).

[21] J. Jiang, J. Zou, M.N. Anjum, J. Yan, L. Huang, Y. Zhang, J. Chen, Synthesis and characterization of wafer-like BiFeO3with efficient catalytic activity, Solid State Sci. 13 (2011) 1779–1785.

[22] S.J.A. Moniz, R. Quesada-Cabrera, C.S. Blackman, J. Tang, P. Southern, P.M. Weaver, C.J. Carmalt, A simple, low-cost CVD route to thin films of BiFeO3for efficient water photo-oxidation, J. Mater. Chem. A. 2 (2014) 2922–2927.

[23] H.-Y. Xu, L.-C. Wu, H. Zhao, L.-G. Jin, S.-Y. Qi, Synergic effect between adsorption and photocatalysis of metal-free g-C3N4 derived from different precursors, PLoS One 10 (2015) e0142616.

[24] S. Kazhugasalamoorthy, P. Jegatheesan, R. Mohandoss, N.V. Giridharan, B. Karthikeyan, R.J. Joseyphus, S. Dhanuskodi, Investigations on the properties of pure and rare earth modified bismuth ferrite ceramics, J. Alloy. Comp. 493 (2010) 569–572.

[25] N. Fiol, I. Villaescusa, Determination of sorbent point zero charge: usefulness in sorption studies, Environ. Chem. Lett. 7 (2009) 79–84.

[26] S. Bae, S. Kim, S. Lee, W. Choi, Dye decolorization test for the activity assessment of visible light photocatalysts: realities and limitations, Catal. Today 224 (2014) 21–28.

[27] A. Salhi, A. Aarfane, S. Tahiri, L. Khamliche, M. Bensitel, Study of the photocatalytic degradation of methylene blue dye using titanium-doped hydroxyapatite, Mediterr. J. Chem. 4 (2015) 59–67 2015.

[28] Y. Liu, I. Zhitomirsky, Electrochemical supercomputer based on multifarious BiMn2O5, J. Power Sources 284 (2015) 377–382.

[29] F. Majid, S.T. Mirza, S. Riaz, S. Naseem, Sol-gel synthesis of $BiFeO_3$ nanoparticles, Mater. Today: Proceedings 2 (2015) 5293–5297.

[30] S. Godara, N. Sinha, G. Ray, B. Kumar, Combined structural, electrical, magnetic and optical characterization of bismuth ferrite nanoparticles synthesized by auto combustion route, J. Asian Ceram. Soc. 2 (2014) 416–421.

[31] A. Manzoor, A.M. Afzal, M. Umair, A. Ali, M. Rizwan, M.Z. Yaqoob, Synthesis and characterization of Bismuth ferrite (BiFeO3) nanoparticles by solution evaporation method, J. Magn. Magn. Mater. 393 (2015) 269–272.